Influence of hydrogen on strain localization and fracture behavior in Al-Zn-Mg-Cu aluminum alloys

Su, Hang
Department of Mechanical Engineering, Kyushu University

Toda, Hiroyuki
Department of Mechanical Engineering, Kyushu University

Masunaga, Ryohei
Department of Mechanical Engineering, Kyushu University

Shimizu, Kazuyuki
Department of Mechanical Engineering, Kyushu University

他

出版情報：Acta Materialia. 159, pp.332-343, 2018-10-15. Elsevier B.V.
バージョン：
権利関係：

Figures and tables

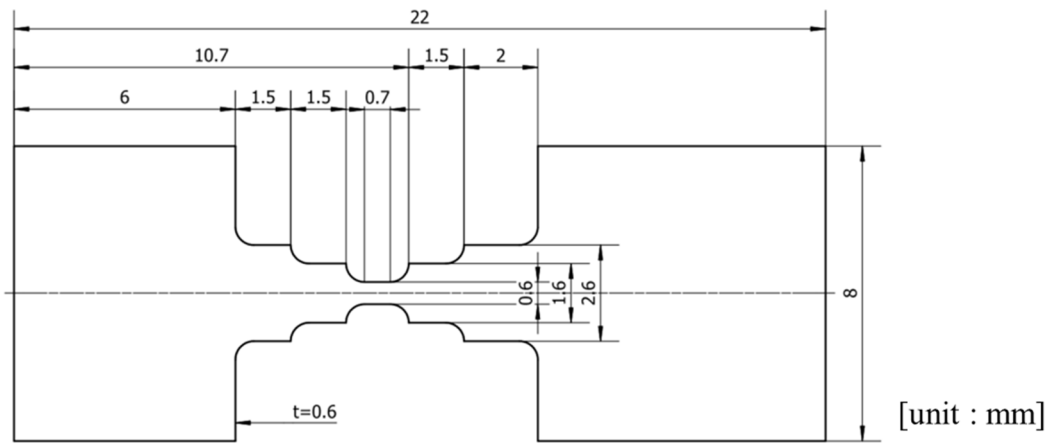

Fig. 1 Geometry of an in-situ tensile test specimen

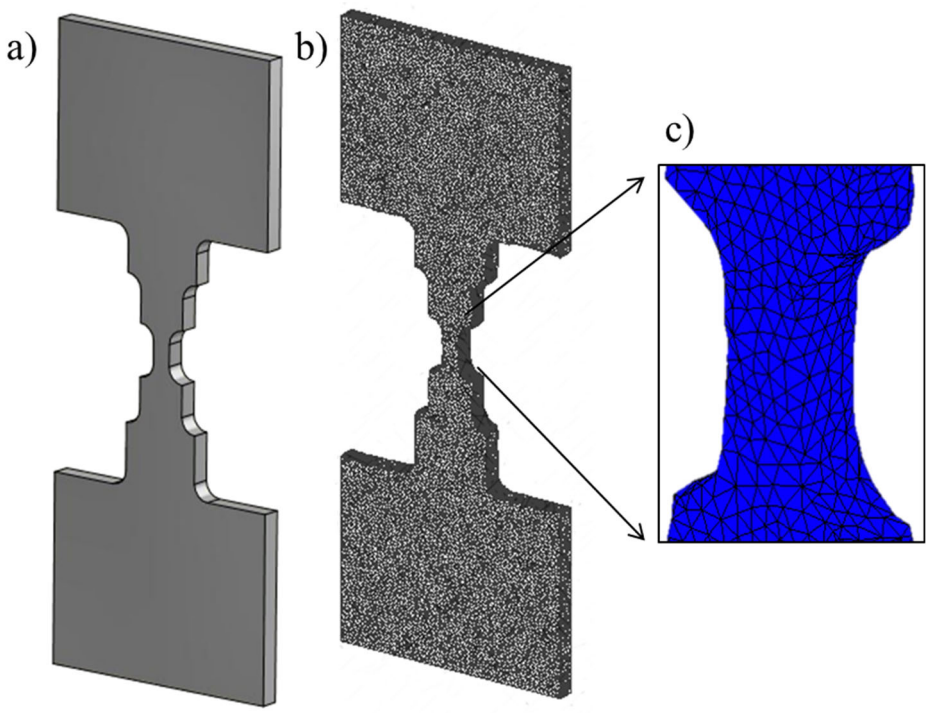

Fig. 2 Procedure to obtain a 3D FE model; a) 3D rendered image of an in-situ tensile test specimen, b) meshing result and c) magnified views of meshing in the gauge of the specimen

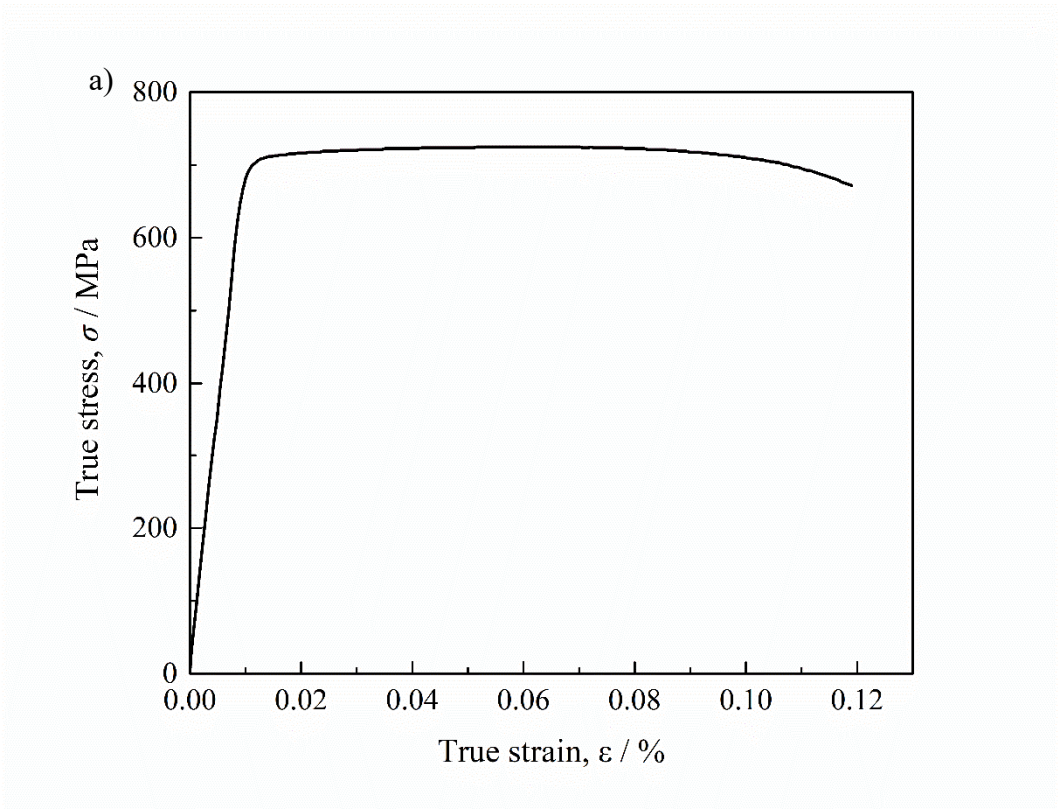

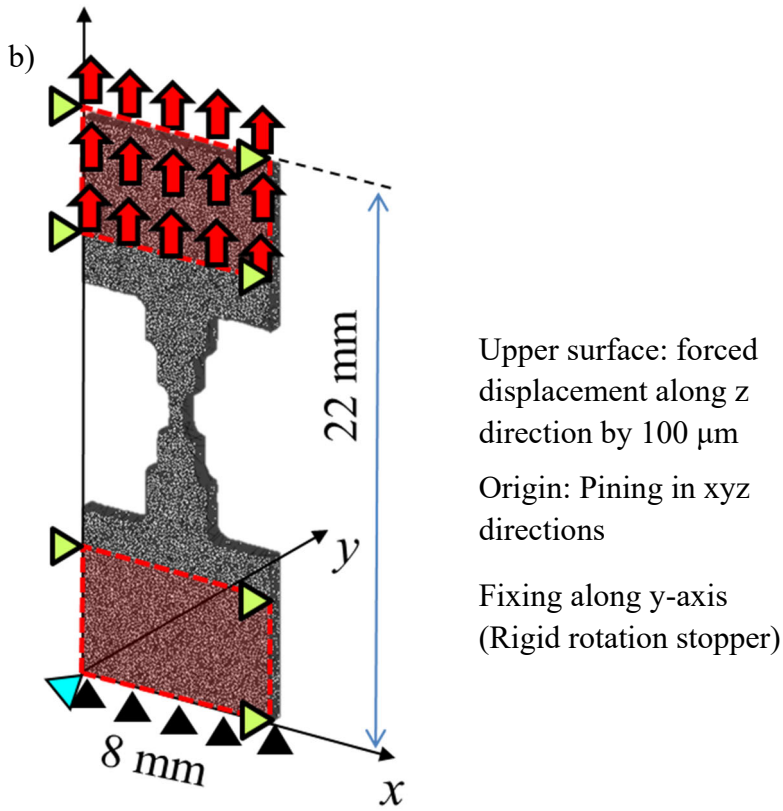

Fig. 3 Schematic illustration of the FEM simulations; a) Plastic constitutive behavior of the material and b) Typical boundary condition for FEM simulations

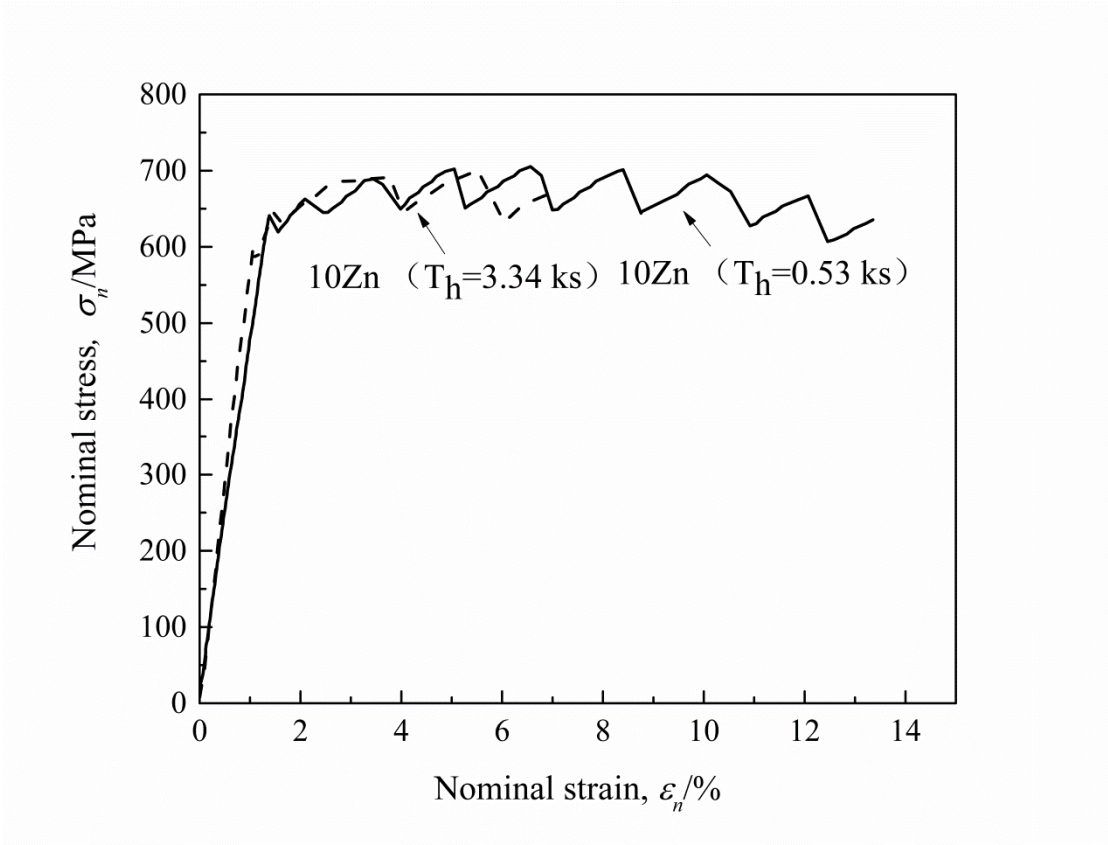

Fig. 4 Stress-strain curves for the in-situ tensile tests

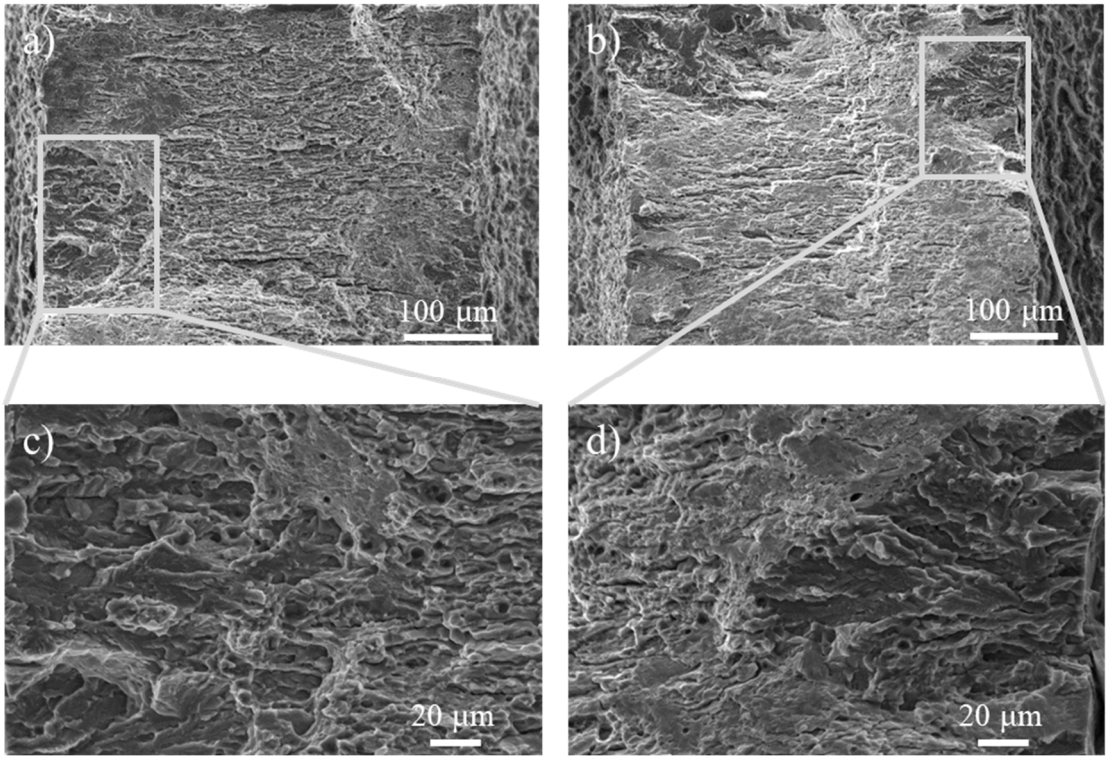

Fig. 5 Fracture surfaces after the in-situ tensile tests; a) 10Zn (T_h=0.53 ks) specimen, b) 10Zn (T_h=3.34 ks) specimen, c) magnified views of the quasi-cleavage crack in 10Zn (T_h=0.53 ks) specimen and d) magnified views of the quasi-cleavage crack in 10Zn (T_h=3.34 ks) specimen

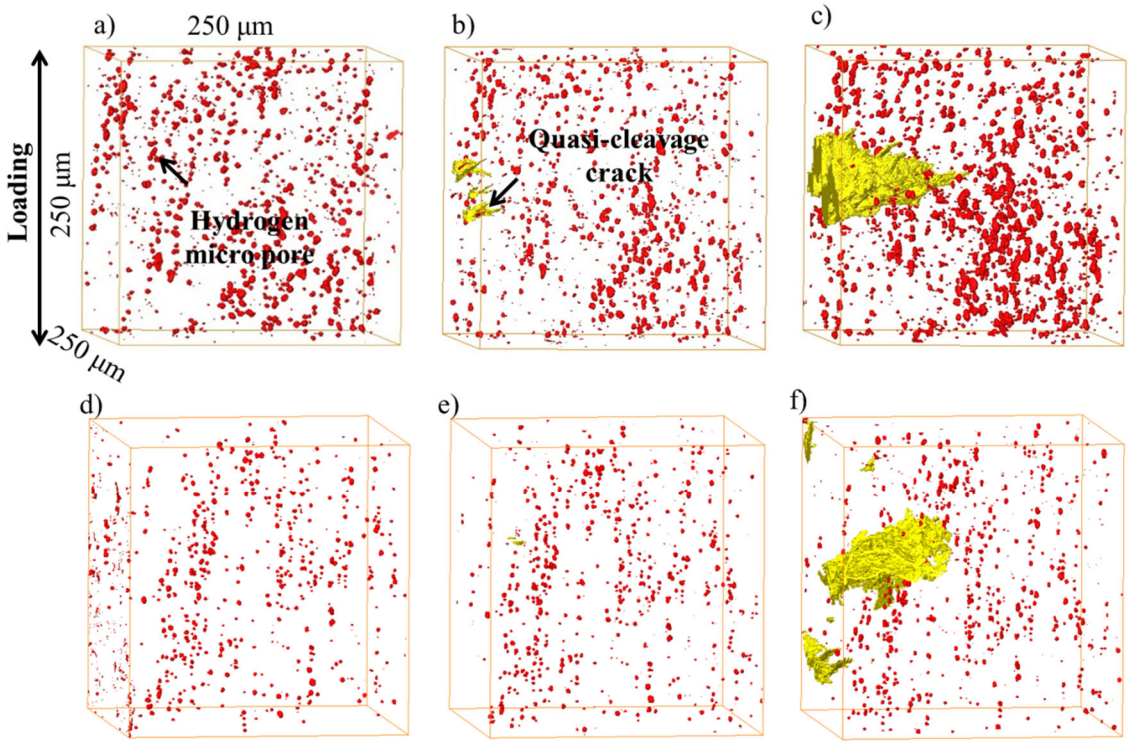

Fig. 6 4D observations of the initiation and propagation of the quasi-cleavage crack in 10 Zn (T_h=0.53ks) under different applied strains; a) ε_a = 0.0 %, b) ε_a = 8.3 % and c) ε_a = 12.0 % and that in 10 Zn (T_h=3.34ks) under different applied strains; a) ε_a = 0.0 %, b) ε_a = 1.5 % and c) ε_a = 5.5 %. Hydrogen micro pores are shown in red and the quasi-cleavage crack is shown in yellow

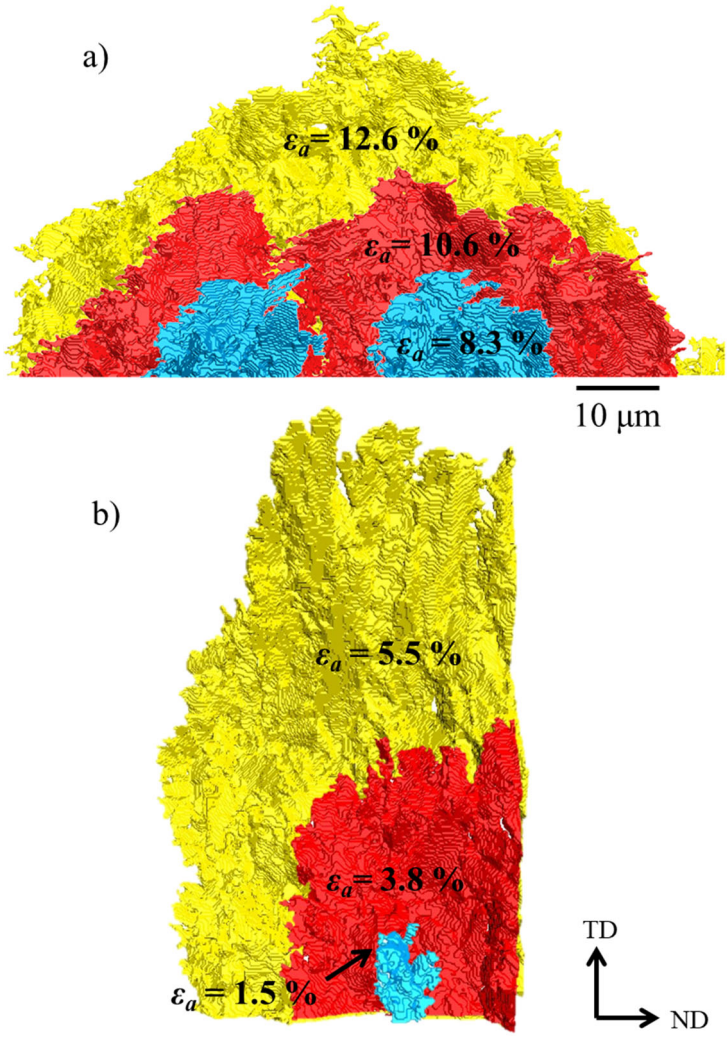

Fig. 7 3D rendered images of a quasi-cleavage crack under different applied strains; a) the quasi-cleavage crack in 10 Zn (T_h=0.53ks) specimen, b) the quasi-cleavage crack in 10 Zn (T_h=3.34ks) specimen

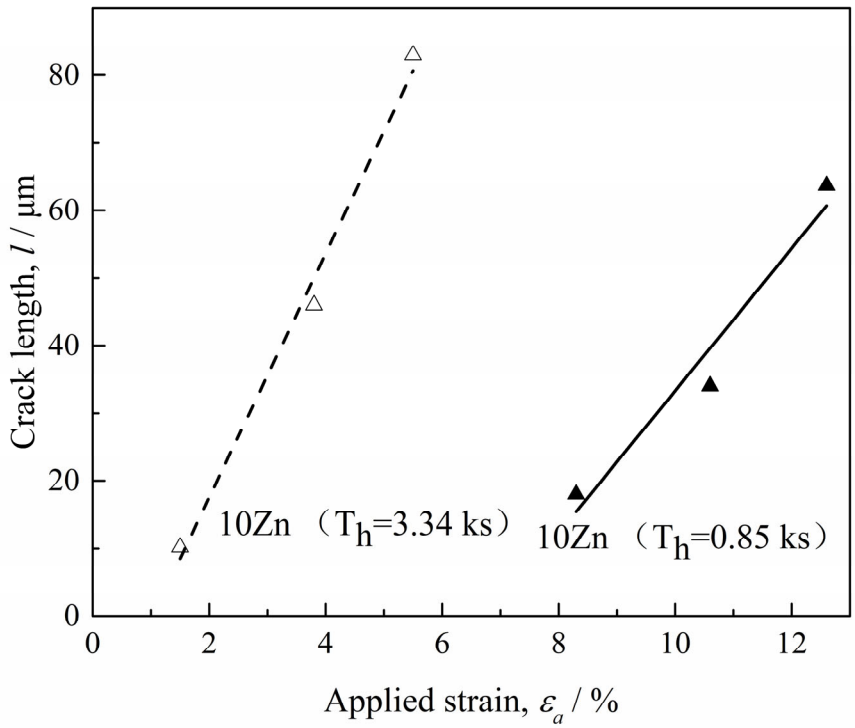

Fig. 8 Growth rates ($dl/d\varepsilon_a$) of the quasi-cleavage cracks during the in-situ tensile tests

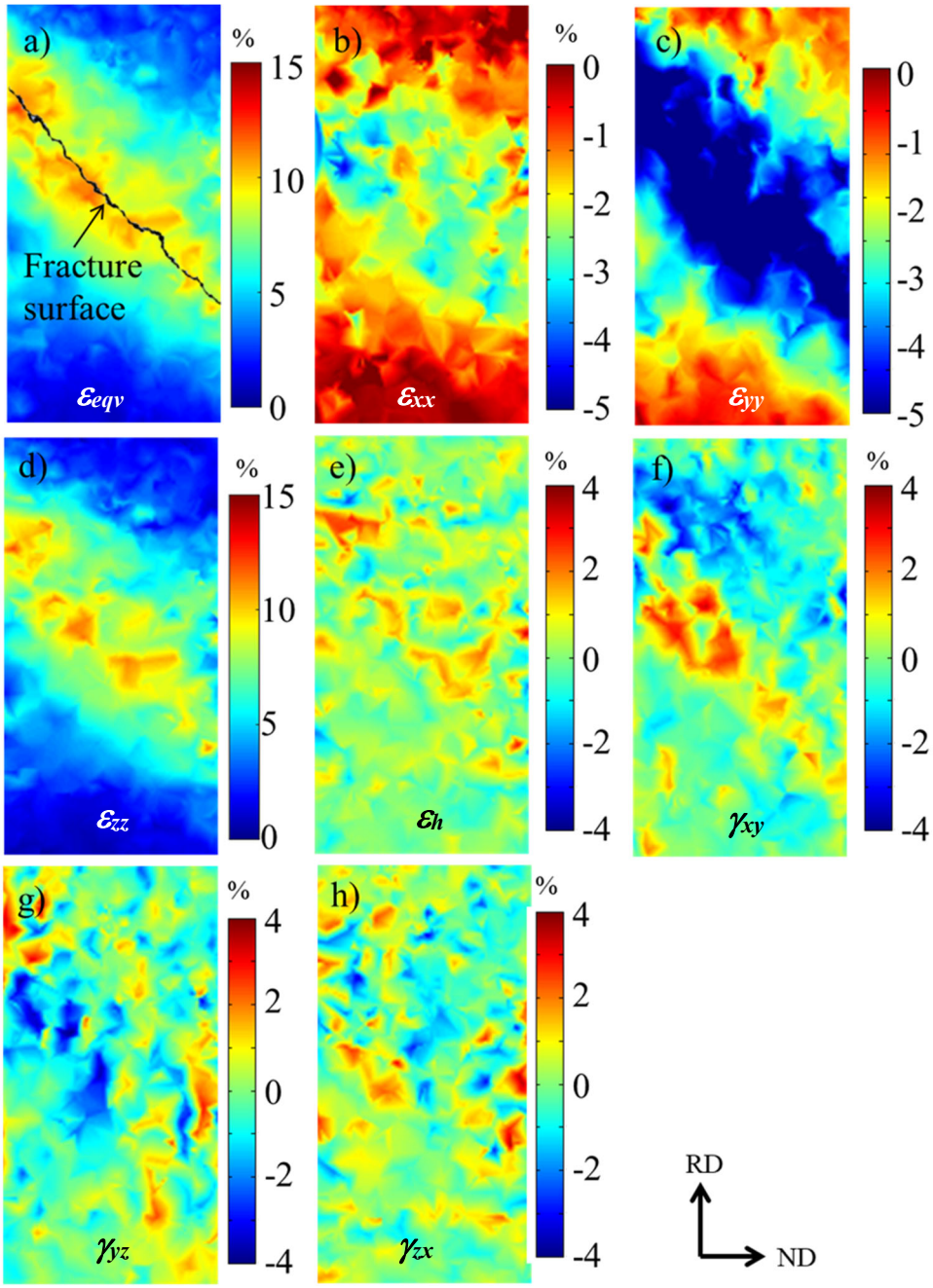

Fig. 9 Strain maps on a y-z (RD-ND) virtual cross-section of 10 Zn (T_h=3.34ks). Plastic strain is calculated between applied strain, ε_a, of 1.1 and 5.5 %. Plotted are: a) equivalent strain, ε_{eq}; b) normal strain in the x (TD) direction, ε_{xx}; c) normal strain in the y (ND) direction, ε_{yy}; d) normal strain in the z (RD) direction, ε_{zz}; e) hydrostatic strain, ε_h; f)shear strain in the x-y direction, γ_{xy}; g) shear strain in the y-z direction, γ_{yz} and h) shear strain in the x-z direction, γ_{xz}

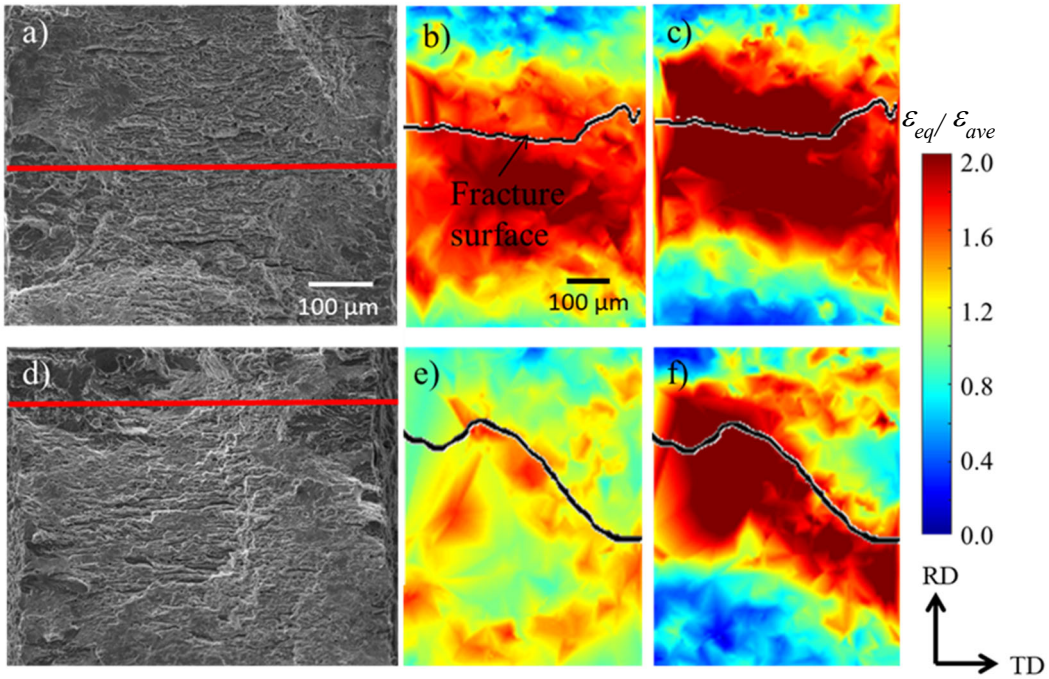

Fig. 10 Representation of the normalized equivalent strain distribution (ε_{eq} / ε_{ave}) ahead of the quasi-cleavage crack tip; a) Fracture surface of 10 Zn (T_h=0.53 ks) and extracted x-z cross section used for b) and c) is marked as red line, b) normalized equivalent strain map is calculated between ε_a of 5.1 and 8.4%, c) normalized equivalent strain map is calculated between ε_a of 8.4 and 12.1%, d) Fracture surface of 10 Zn (T_h=3.34ks) and extracted x-z cross section used for e) and f) is marked as red line, e) normalized equivalent strain map is calculated between ε_a of 0 and 3.8% and f) normalized equivalent strain map is calculated between ε_a of 3.8 and 5.5 %. Fracture surface is shown as the blackline in b), c), e) and f).

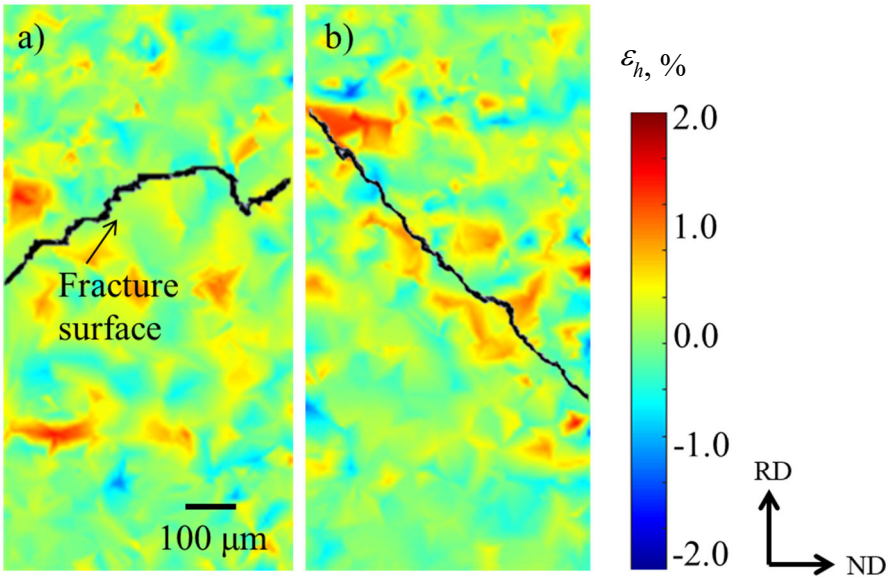

Fig. 11 Hydrostatic strain (ε_h) distribution viewed on the y-z (RD-ND) cross-section under different test conditions. a) hydrostatic strain map calculated between ε_a of 2.1 and 6.8 % in 10 Zn (T_h=0.53ks), b) hydrostatic strain map calculated between ε_a of 1.1 and 5.5 % in 10 Zn (T_h=3.34 ks).

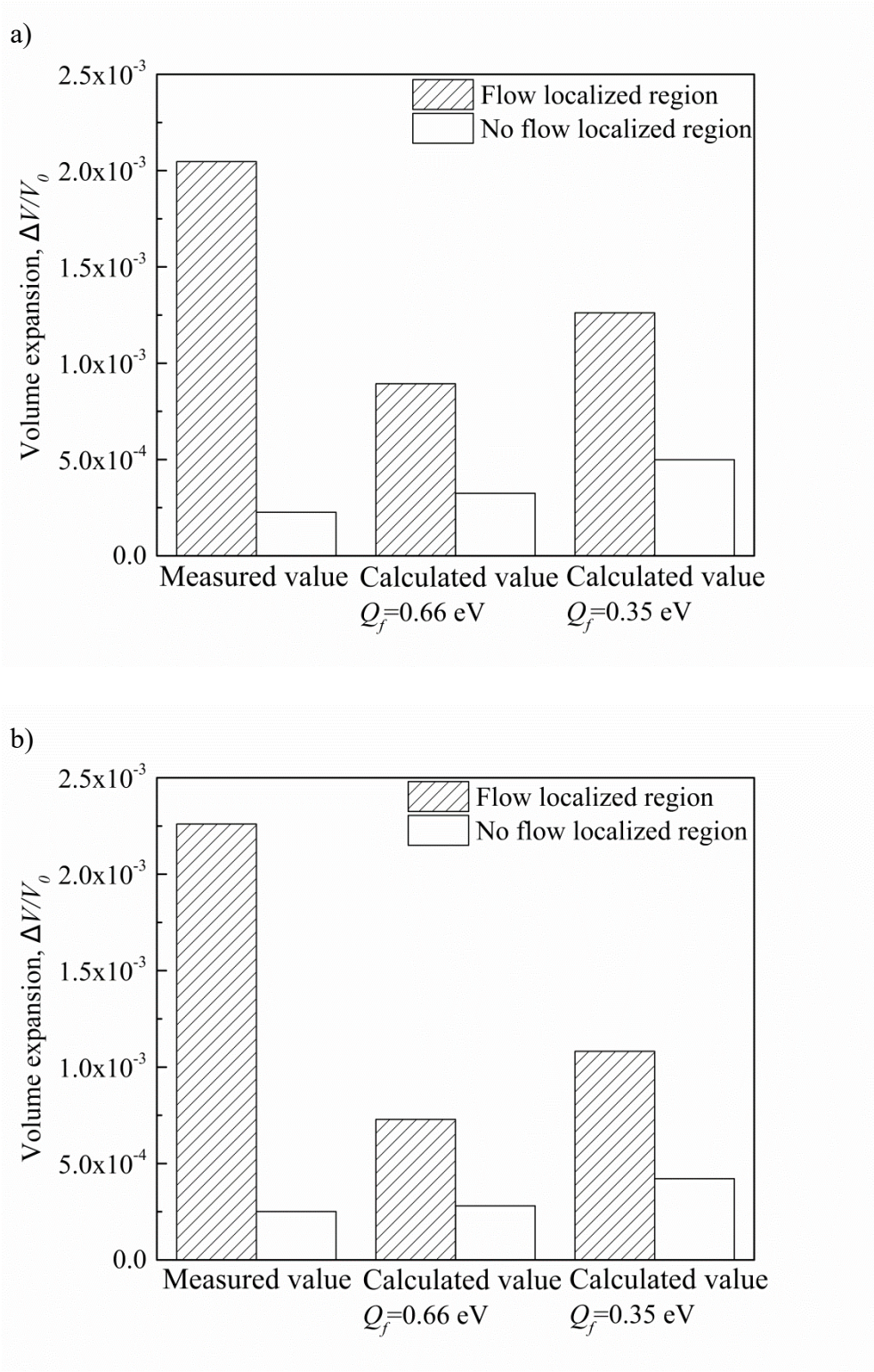

Fig. 12 Comparisons of total vacancy concentration between the measured value and theoretical calculation. a) is calculated between εa of 2.1 and 6.8 % in 10 Zn (T_h=0.53ks), b) is calculated between εa of 1.1 and 5.5 % in 10 Zn (T_h=3.34 ks)

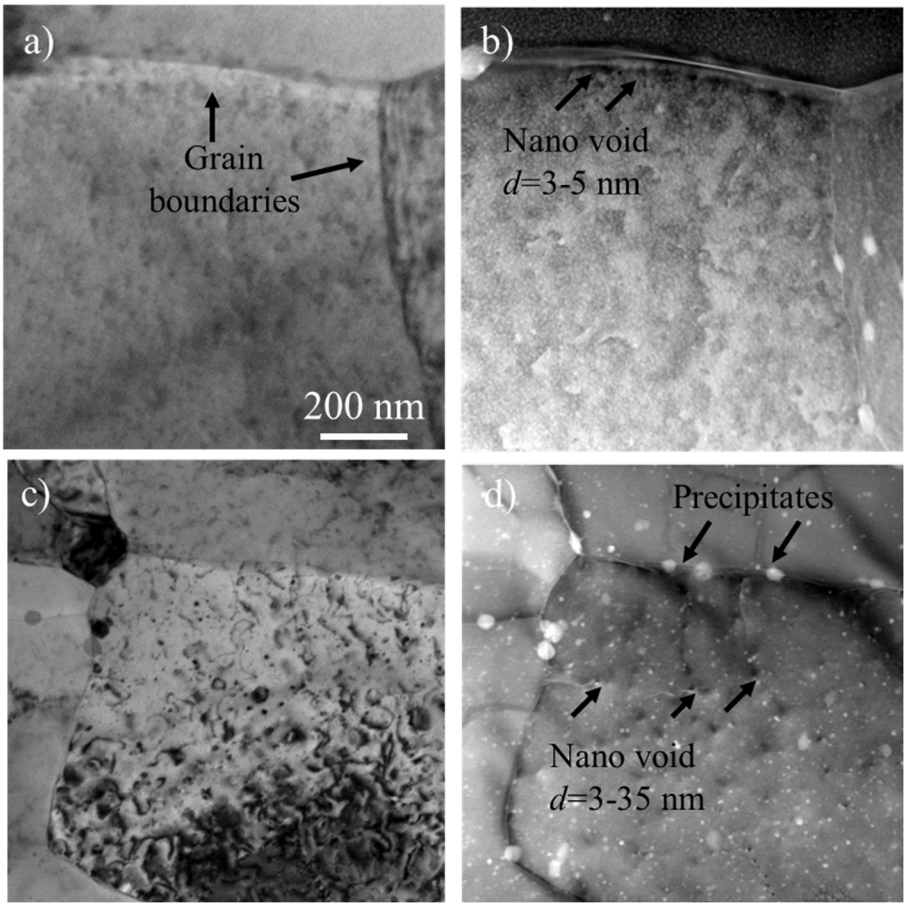

Fig. 13 Observations of nano voids in Al-Zn-Mg-Cu aluminum alloys at different applied strains; a) is the bright-field image of the identical cross-section as in b) at the unloading state b) HAADF-STEM image and nano voids are marked by the black arrows, c) is the bright-field image of the identical cross-section as in d) at an applied strain, ε_a, of 5 %, d) HAADF-STEM image and nano voids are marked by the black arrows.

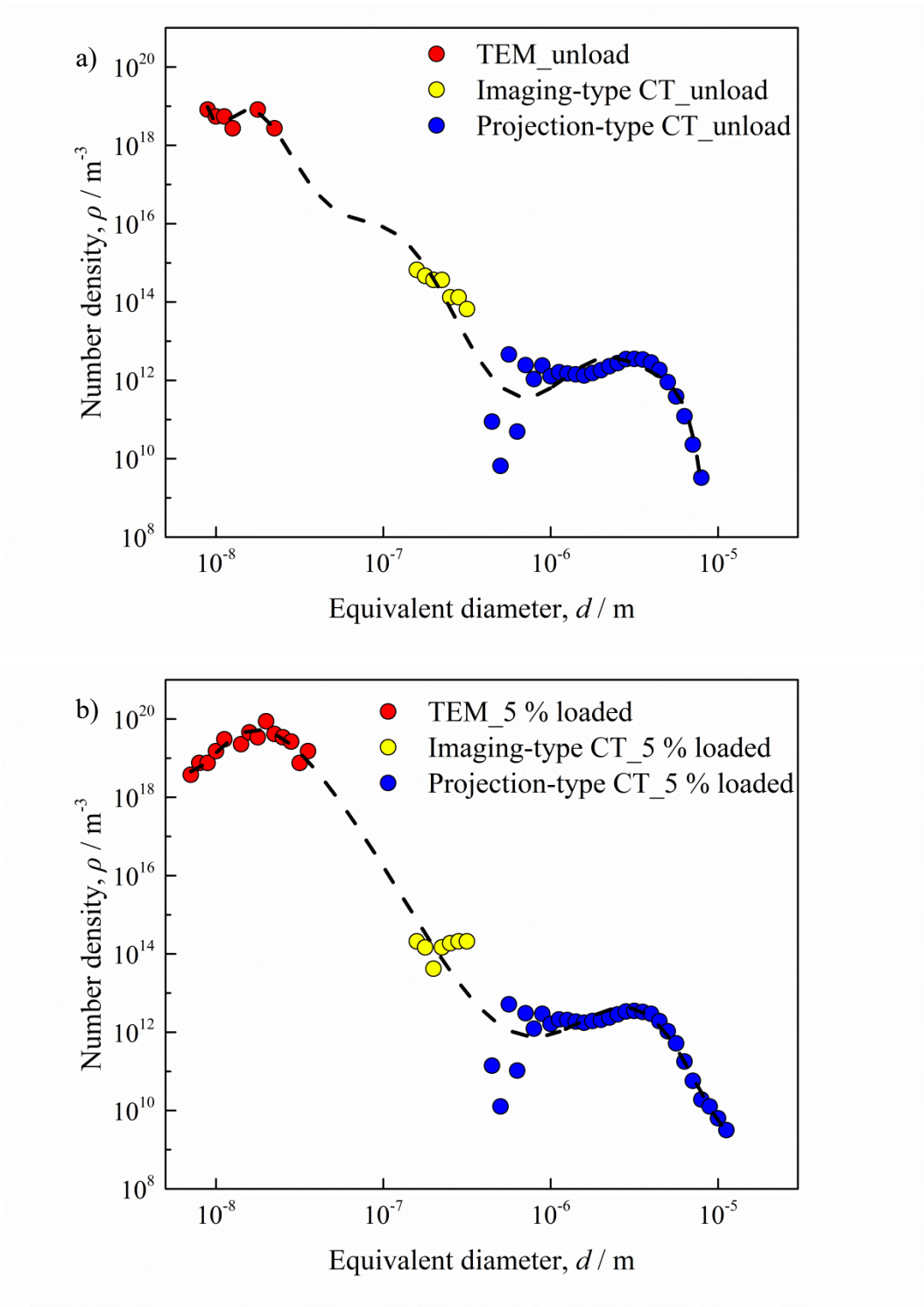

Fig. 14 Changes in the number density and size of nano voids and hydrogen micro pores under different applied strain levels in Al-Zn-Mg-Cu aluminum alloys; a) is at unloading state and b) is at an applied strain, ε_a, of 5 %

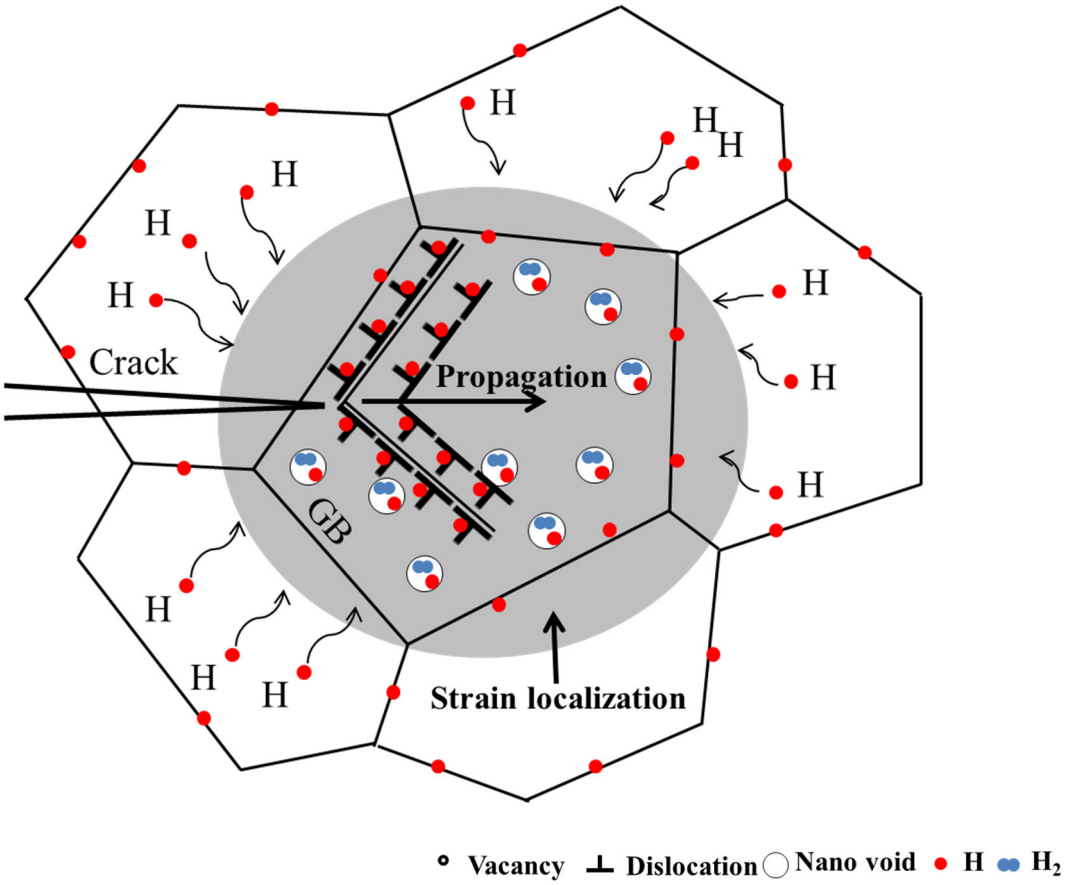

Fig. 15 Schematic illustration of the influence of nano voids on hydrogen partitioning and related crack propagation in a strain localization region